

PAPER • OPEN ACCESS

## Structural modal identification and health monitoring of building structures using self-sensing cementitious composites

To cite this article: Siqi Ding *et al* 2020 *Smart Mater. Struct.* **29** 055013

View the [article online](#) for updates and enhancements.

# Structural modal identification and health monitoring of building structures using self-sensing cementitious composites

Siqi Ding<sup>1</sup> , You-Wu Wang<sup>1</sup> , Yi-Qing Ni<sup>1</sup>  and Baoguo Han<sup>2</sup> 

<sup>1</sup>Department of Civil and Environmental Engineering, The Hong Kong Polytechnic University, Hung Hom, Kowloon, Hong Kong, People's Republic of China

<sup>2</sup>School of Civil Engineering, Dalian University of Technology, Dalian 116024, People's Republic of China

E-mail: [ceyqni@polyu.edu.hk](mailto:ceyqni@polyu.edu.hk)

Received 12 November 2019, revised 6 February 2020

Accepted for publication 25 February 2020

Published 31 March 2020



CrossMark

## Abstract

Recently self-sensing cementitious composite has demonstrated its strong potentiality for structural health monitoring of civil infrastructures because of its low-cost, long-term stability and compatibility with concrete structures. In this paper, we propose novel hybrid nanocarbon materials engineered cement-based sensors (HNCSs) with high-sensitivity, which are fabricated with self-sensing cementitious composites containing electrostatic self-assembled CNT/NCB composite fillers. The mechanical property and sensing performance of the HNCSs are pre-characterized under static and dynamic compressive loadings. The HNCSs are then integrated into a five-story building model via custom-made clamps to verify the feasibility for dynamic response measurements. Results show that the developed sensors have satisfactory mechanical property and excellent pressure-sensitive reproducibility and stability. With clamps holding on the building model, the HNCSs perform satisfactorily under sinusoidal excitations in the frequency range from 2 to 40 Hz. In addition, the modal frequencies and their changes of the building model caused by 'damage' simulated through adding additional masses identified by the HNCSs are favorably consistent with the counterparts acquired by accelerometers and strain gauges, indicating that the developed HNCSs have great potential for structural modal identification and damage detection applications.

Keywords: self-sensing, cement, sensor, carbon nanotube, modal identification, structural health monitoring

(Some figures may appear in colour only in the online journal)

## 1. Introduction

Structural health monitoring (SHM) technology has nowadays received significant attention in civil engineering as it can be implemented on civil structures such as long-span bridges and high-rise buildings to continuously monitor and

evaluate the symptoms of operational incidents, anomalies and possible damage/deterioration, thus providing evidences for safety assessment and enabling the evaluation of effectiveness of maintenance and rehabilitation activities. In line with SHM systems, vibration-based damage detection methods have been extensively used for structural health and condition assessment, with the underlying premise that changes in the physical properties (such as mass, stiffness and damping) that characterize structural damage or degradation would lead to changes in the modal parameters (such as natural frequencies, mode shapes and modal damping). As



Original content from this work may be used under the terms of the [Creative Commons Attribution 4.0 licence](https://creativecommons.org/licenses/by/4.0/). Any further distribution of this work must maintain attribution to the author(s) and the title of the work, journal citation and DOI.

such, damage or degradation can be identified by detecting the changes in dynamic characteristics of the structure concerned [1–9]. While a variety of sensors such as accelerometer, linear variable differential transformer, deflection gauge, dynamic strain sensor, moving test vehicle, global positioning system (GPS) and digital video camera have been successfully employed to monitor structural dynamic responses and identify modal properties in a tremendous amount of research and real SHM projects [10–17], the recent advancement in smart materials opens up new avenues to develop more sensing devices for different application purposes and demands.

In the recent years, there has been an enormous growth in multidisciplinary research of self-sensing cementitious composites. The self-sensing cementitious composites are fabricated by adding conductive fillers such as carbon fiber, steel fiber, carbon black, carbon nanotube (CNT), graphene and nickel powder into cement matrix, forming extensive conductive networks inside. In this manner, the self-sensing cementitious composites can transduce strain (or deformation), stress (or external force), temperature, crack, and damage into the change in electrical signal such as electrical resistance, capacitance, current and voltage if the conductive network inside is changed under deformations or effects of surrounding environment, i.e. pressure-sensitivity [18–25]. In addition to the self-sensing property, the self-sensing cementitious composites offer a range of advantages including high mechanical properties, low cost, high durability and good compatibility with concrete structures, thus making them highly attractive to a wide variety of applications, such as distributed strain-sensing elements for large-scale concrete structures [26] and ‘smart bricks’ for earthquake-induced damage detection and localization in masonry structures [27].

Since the pioneering work made by Chen and Chung in early 1990s [28] who discovered self-sensing cementitious composites incorporating short carbon fibers, a great deal of research has been carried out on fabrication, sensing performance and mechanism recognitions of self-sensing cementitious composites with various conductive fillers, in particular with CNTs due to their extremely high tensile strengths, high moduli, large aspect ratios, low densities, good chemical and environmental stabilities, and high thermal and electrical conductivities [29, 30]. For example, Li *et al* [19, 31] introduced covalently treated and untreated CNTs into cementitious composites with the aid of special ultrasonic treatment and found that both mechanical properties and electrical conductivities of the cementitious composites are improved. Yu *et al* [32] investigated the self-sensing property of cementitious composites with different CNT contents. Experimental results indicated that the electrical resistance of the cementitious composites altered synchronously with the compressive stress level, and a higher CNT content could improve the sensitivity of the cementitious composite stress response. Han *et al* [33] conducted an experimental study on the self-sensing property of cementitious composites with 0.1% and 0.5% of CNTs and proposed two measurement methods for self-sensing responses of the cementitious composites with CNTs. The experimental results indicated that the

self-sensing cementitious composites with CNTs have both resistance and capacitance characteristics. Cui *et al* [34] compared the effects of 12 different types of commercially available CNTs on the performance and microstructure of self-sensing cementitious composites and revealed that the CNT reinforcement effect can be attributed to extensively distributed meshwork in cement matrix, crack bridging, fiber pull-out effect, lowering orientation index of CH crystal in hydration products and decreasing cement hydration degree. Based on two mechanisms of electron hopping and conductive networks, García-Macías *et al* [35] proposed a micromechanics model of self-sensing cementitious composites with CNTs by the consideration of waviness and uniform dispersions of CNTs and revealed that the origin of self-sensing property is attributed to strain-induced changes in the volume fraction, filler reorientation and changes in the tunneling resistance variation of the inter-particle distance. However, the applications of self-sensing cementitious composites with CNTs are still few and most of the studies have focused on the performance of CNT-filled self-sensing cementitious composites in the time domain. Han *et al* [36] investigated the possibility of using CNT-filled self-sensing cementitious composites for traffic detection. Howser *et al* [37] demonstrated a damage detection approach in concrete beams fabricated with CNT-filled self-sensing cementitious composites under reversed cyclic loads. The damage was clearly detected by reading the measured electrical resistance. Downey *et al* [38, 39] introduced a resistor mesh model capable of damage detection within structural elements made of self-sensing cementitious composites with CNTs, which has the potential of enabling real-time detection, localization and quantification of crack-type damage in full-scale concrete structures.

As aforementioned, vibration-based damage detection methods in SHM mainly use the changes in measured modal properties and their derivatives/variants to infer the symptoms of structural damage and/or deterioration. Yet there is a paucity of research on the development of CNT-filled self-sensing cementitious composites for monitoring of structural vibration and dynamic characteristics in line with vibration-based damage detection [40]. Also, an important issue that must be handled properly in the application of CNT-filled self-sensing cementitious composites for vibration sensing is the tendency of CNTs to agglomerate in clusters due to the large surface area of CNTs promoting the appearance of van der Waals’ attraction forces [41]. Recently, the authors have synthesized nano carbon black (NCB) onto CNT via electrostatic self-assembly to form CNT/NCB composite fillers, which could address the dispersion issue of CNTs in cementitious materials, thus endowing stable and sensitive self-sensing property to cementitious composites even at a low content of CNT/NCB composite fillers and greatly facilitating the fabrication process in large-scale industrial production [42].

In this study, self-sensing cementitious composites filled with CNT/NCB composite fillers are fabricated to develop hybrid nanocarbon materials engineered cement-based sensors (HNCSs) for structural modal identification targeted at

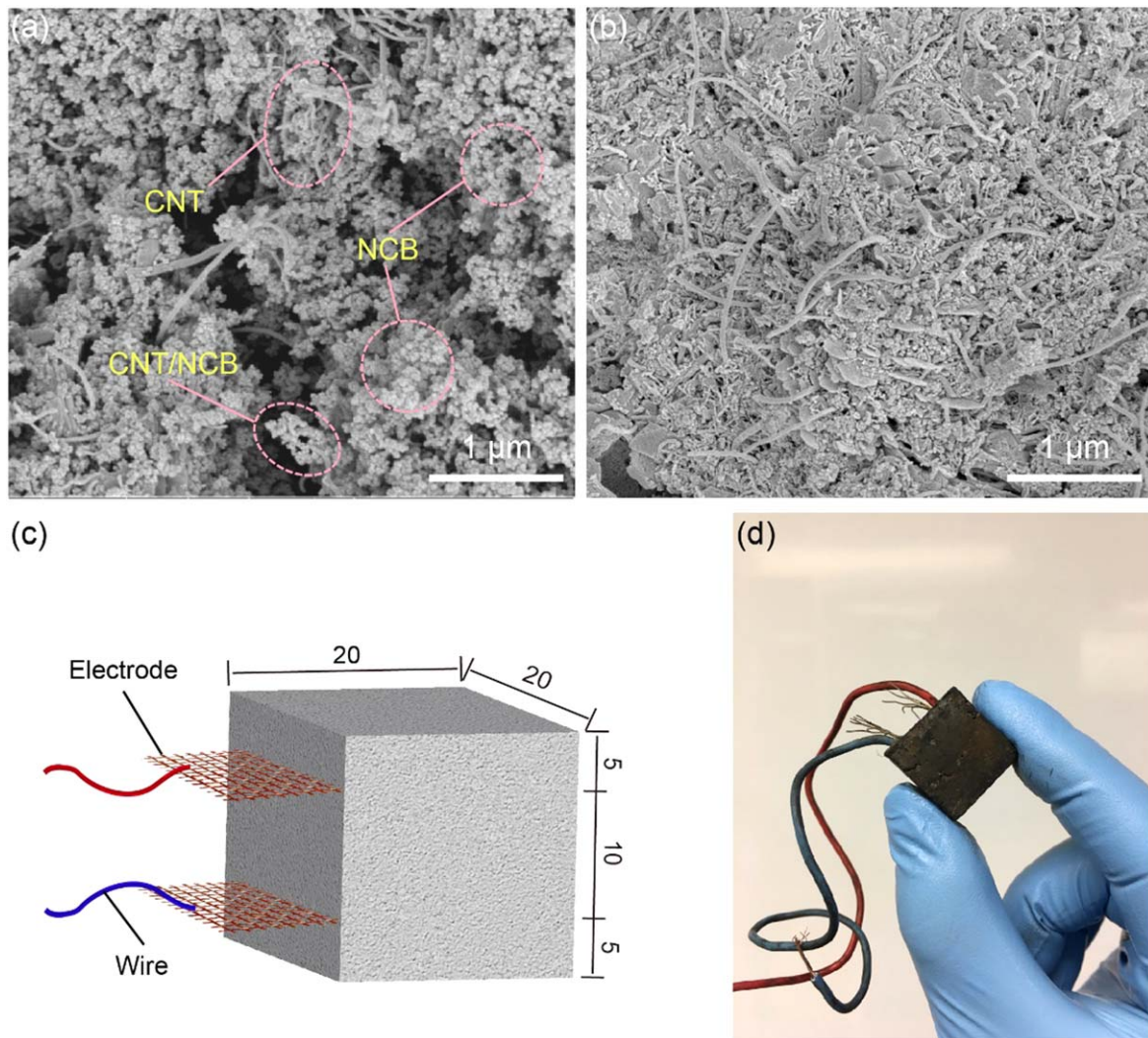


**Figure 1.** (a) SEM image of CNT/NCB composite fillers; (b) CNT/NCB composite fillers uniformly distributed in cement matrix forming extensive conductive network; (c) Dimension and electrode arrangement of HNCS; (d) Photograph of a HNCS specimen.

**Table 1.** Physical properties of CNT/NCB composite fillers.

| Properties  | Description/value |
|---|-------------------|
| Mass ratio of CNTs/NCBs to hybrid/wt%                     | 40/60             |
| Shape   | Grape clusters    |
| Specific gravity/ $\text{g cm}^{-3}$                      | 2.0               |
| Specific surface area/ $\text{m}^2 \text{g}^{-1}$         | 65–75             |
| Electrical resistivity/ $\Omega \text{ cm}$               | $10^{-3}$         |
| Outer diameter of CNTs/nm                                 | >50               |
| Length of CNTs/ $\mu\text{m}$                             | 10–20             |
| Specific surface area of CNTs/ $\text{m}^2 \text{g}^{-1}$ | >40               |
| Tap density of CNTs/ $\text{g cm}^{-3}$                   | 0.18              |
| Particle size of NCBs/nm                                  | 23                |
| Specific surface area of NCBs/ $\text{m}^2 \text{g}^{-1}$ | 125               |

vibration-based damage detection. The mechanical property and sensing performance of the HNCSs are first explored under static and dynamic compressive loadings in lab tests. Afterwards, the dynamic performance of the HNCSs deployed on a five-story building model is experimentally

investigated. Finally, the feasibility of using the dynamic responses from the HNCSs for modal-based damage detection is verified and compared with that using commercially available accelerometers and strain gauges.

## 2. Experimental procedure

### 2.1. Sensor fabrication

The HNCSs are fabricated by cement, fly ash, water, super-plasticizer and CNT/NCB composite fillers. The CNT/NCB composite fillers purchased from Chengdu Institute of Organic Chemistry Co., Ltd. are employed as conductive fillers. The SEM (NanoSEM 450, FEI Ltd., USA) picture of their self-assembled botryoid structure can be viewed in figure 1(a). This structure enables effective dispersion of both CNTs and NCBs in cement matrix, thus offering superior electrical conductivity and pressure-sensitivity [42]. Table 1 summarizes the physical properties of the CNT/NCB composite fillers. The ASTM Type I normal Portland cement

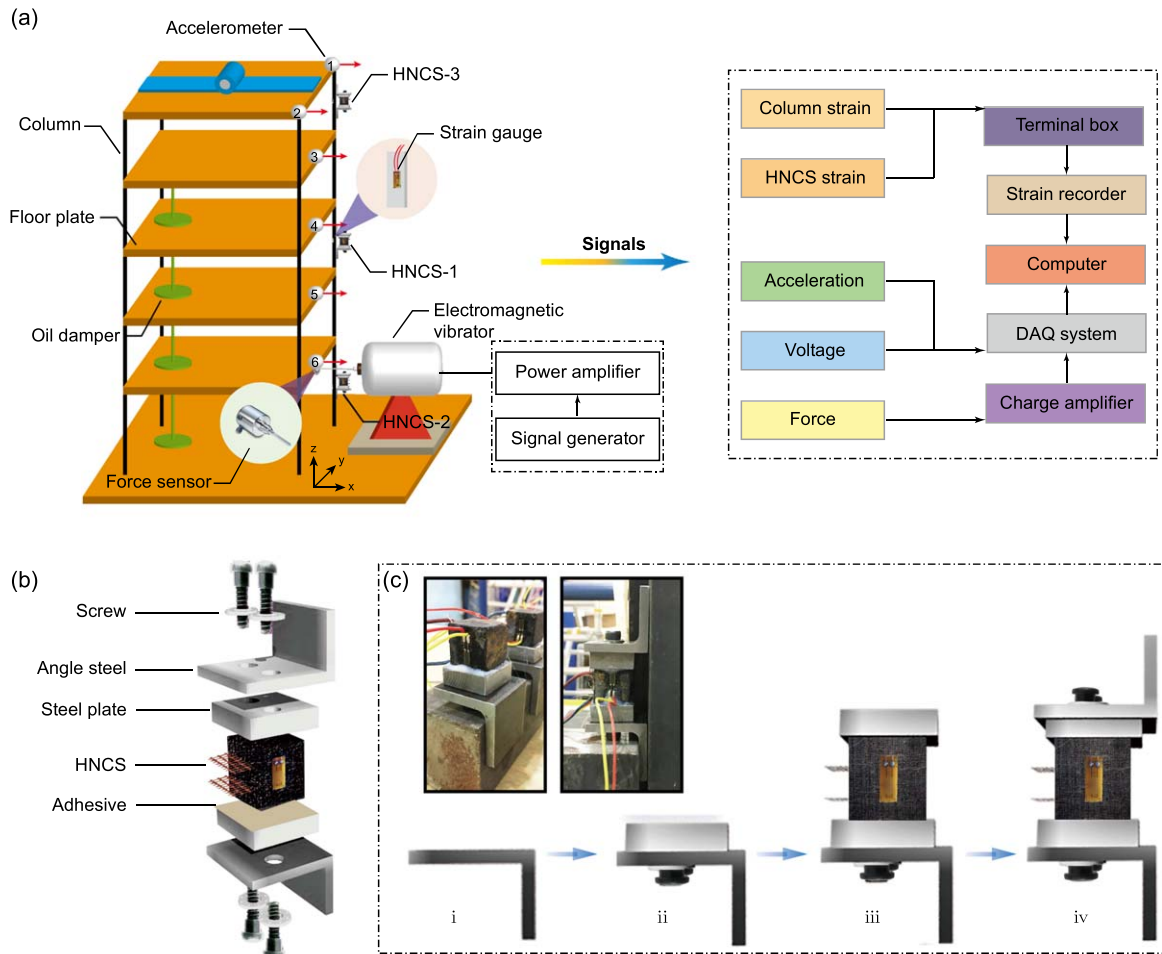


**Figure 2.** (a) Schematic diagram of the experimental setup and flowchart for signal acquisition; (b) schematic illustration of the clamp used for fixing the HNCS on the building model; (c) assembly process of the HNCS clamp: (i) Put a L-shaped angle steel vertically; (ii) Connect a steel plate with the angle steel with a pair of screws and paint a modified acrylic adhesive layer on the surface of the steel plate; (iii) Position a HNCS on the adhesive layer carefully for 10 min (insert: left) and then place the flat side painted with an adhesive layer of another steel plate on the HNCS for 10 min; (iv) Fix another L-shaped angle steel with the steel plate. Notice: Make sure that the two angle steels are located at the same vertical line (insert: right).

**Table 2.** Mixing proportions of HNCS specimens.

| Cement | Fly ash (wt%) <sup>a</sup> | W/B <sup>b</sup> | CNTs/NCBs (wt%) <sup>c</sup> | Superplasticizer (wt%) <sup>c</sup> |
|--------|----------------------------|------------------|------------------------------|-------------------------------------|
| 1      | 20                         | 0.5              | 6                            | 2                                   |

<sup>a</sup> The amount of fly ash is by weight of cement.

<sup>b</sup> W/B is water to binder ratio. Binder is composed of cement and silica fume.

<sup>c</sup> The amount of CNTs/NCBs and superplasticizer is by weight of binder.

42.5R (Dalian Xiaoyetian Cement Co. Ltd., China) and fly ash (Dalian Huayuan Fly Ash Co., Ltd., China) are used as matrix materials. A polycarboxylate superplasticizer with a solid content of 45% (3310E, Sika Co. Ltd., China) is used to facilitate the workability of the mixtures.

In accordance with the dimension of the five-story building model, the dimension of the HNCSs is fixed at 20 mm × 20 mm × 20 mm (figure 1(c)). Our prior work has demonstrated that due to different transverse deformation under compression, a square specimen has a higher piezoresistive

sensitivity, better accuracy and reproducibility than a rectangular one. In addition, the optimal content of CNT/NCB composite fillers providing the best piezoresistive sensitivity has been determined as 6 wt% of cement [42]. The HNCS specimens are fabricated according to the mixing proportions as listed in table 2. The fabrication process is schematically described as follows. First, the polycarboxylate superplasticizer is added to water and mixed for 20 s in a beaker. Second, the pre-weighted cement and fly ash are poured into the aqueous solution at the same time and mixed for 2 min using a

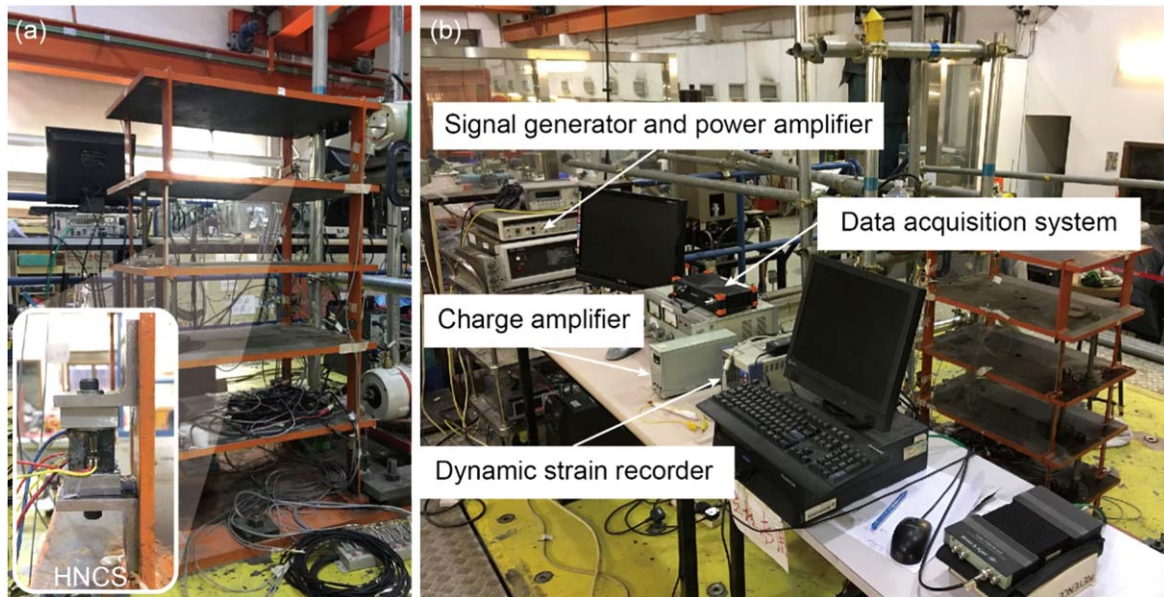


**Figure 3.** Pictures of the experimental setup: (a) five-story building model at The Hong Kong Polytechnic University. Insert: HNCS mounted on the building model; (b) equipment for vibration tests and data acquisition.

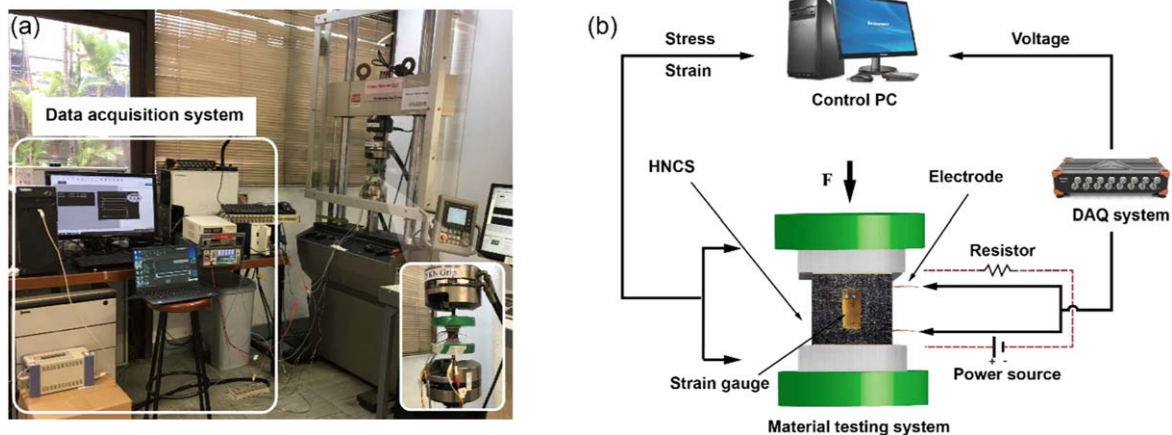


**Figure 4.** Tests on the static and dynamic performance of HNCS: (a) photograph of the testing apparatus; (b) schematic diagram of the testing system.

mechanical stirrer. Then the CNT/NCB composite fillers are gradually added to the mixture and only mechanically mixed for 3 min without using additional dispersion technique. Fourth, the mixture is evenly poured into oiled mold. Two stainless steel electrodes with openings of  $2\text{ mm} \times 2\text{ mm}$  are then embedded in the middle of the specimens at a spacing of 10 mm. Subsequently, the mold is shocked by an electric vibrator for 5 s to eliminate bubbles. Lastly, the specimens after demolding are cured in water at  $20\text{ }^{\circ}\text{C}$  for 28 d. Three specimens named HNCS-1, HNCS-2 and HNCS-3 have been fabricated for the experimental campaign (figure 1(d)). The SEM image of the hardened HNCS sample with CNT/NCB composite fillers is shown in figure 1(b). It can be observed that the CNT/NCB

composite fillers can be uniformly dispersed in cement matrix without using additional dispersion technique.

## 2.2. Experimental setup

To investigate the performance of the devised HNCSs for acquiring dynamic responses for the purpose of structural modal identification and damage detection, a five-story building model is fabricated at the Dynamic Structural Laboratory of The Hong Kong Polytechnic University, as shown in figure 2. The building model consists of five steel floor plates with a size of  $600\text{ mm} \times 400\text{ mm} \times 15\text{ mm}$  and four equal rectangular columns with cross section of

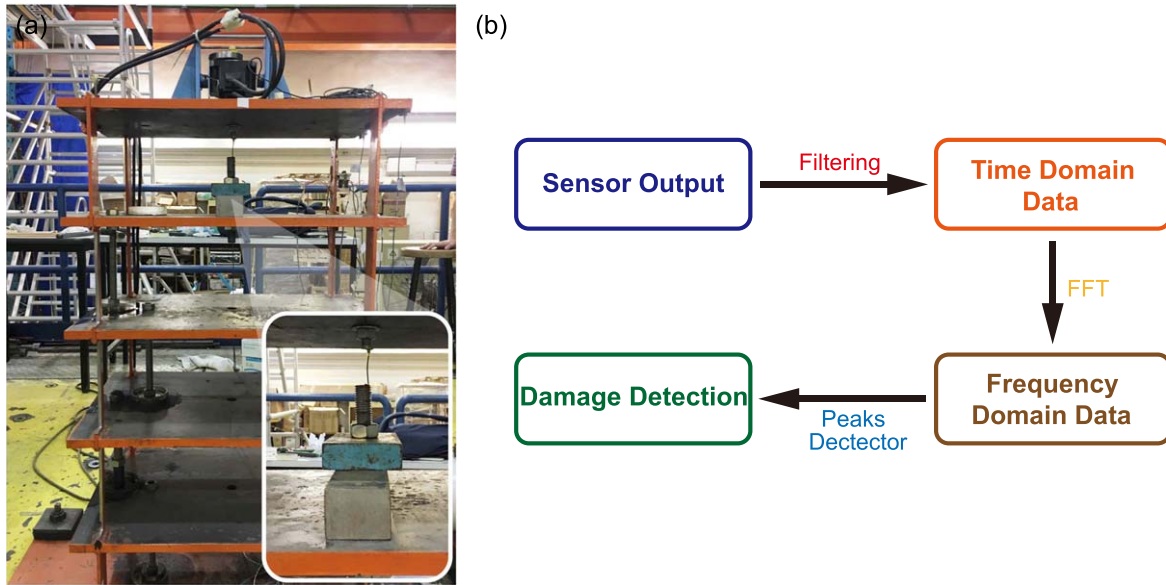


**Figure 5.** (a) Photograph of experimental setup for damage detection. Insert: auxiliary iron brick bolted in the center of floor plate; (b) flowchart of FFT data processing.

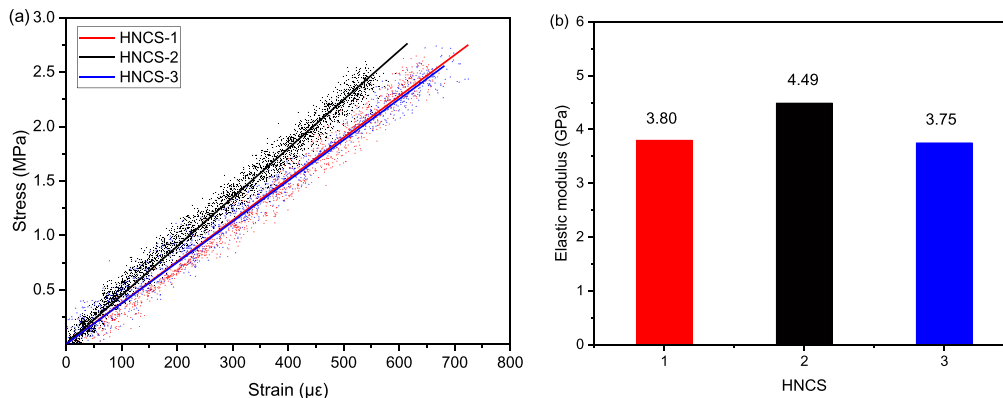


**Figure 6.** Mechanical properties of the HNCSs: (a) relationship between compressive stress and strain of the HNCSs; (b) elastic modulus values of the three HNCSs.

**Table 3.** Electrical resistance and pressure-sensitivity of the three HNCSs.

| HNCS                               | 1                              | 2                              | 3                              |
|------------------------------------|--------------------------------|--------------------------------|--------------------------------|
| Electrical resistance ( $\Omega$ ) | $68.417 \pm 1.324$             | $42.327 \pm 0.707$             | $22.781 \pm 1.449$             |
| Sensitivity (%/MPa)                | $1.73 \pm 1.53 \times 10^{-2}$ | $1.14 \pm 5.13 \times 10^{-3}$ | $2.52 \pm 2.73 \times 10^{-2}$ |
| Voltage (V)                        | 1.08162                        | 1.84469                        | 1.90079                        |

50 mm  $\times$  6 mm. Each floor plate is firmly welded to the four columns in the horizontal direction. The cross section of the columns is configured to make the stiffness of the building model in  $x$ -direction much smaller than that in  $y$ -direction, leading to a shear type deformation. The total height of the model is 1000 mm, with the same height of each story. To increase the structural damping, a series of silicon oil dampers are designed and installed at the floor levels. An electromagnetic vibrator (LDS<sup>®</sup> V406, Brüel & Kjær, Denmark) deployed at the first floor level is used to impose dynamic excitations. The electromagnetic vibrator is controlled by a

third-party control system (Model DS360 Ultra Low Distortion Function Generator, Stanford Research System, USA) to offer different excitation forces. The controller paired with a power amplifier (LDS<sup>®</sup> PA500L, Brüel & Kjær, Denmark) can impart a maximum sine vector force up to 196 N and feature a usable frequency range from 5 to 9000 Hz. As illustrated in figure 2(a), six uniaxial accelerometers (TYPE 4533-B-002, Brüel & Kjær, Denmark) labeled in number are mounted on the building model through permanent magnets to measure the structural acceleration response. Two accelerometers deployed at the 5th floor level make it possible to

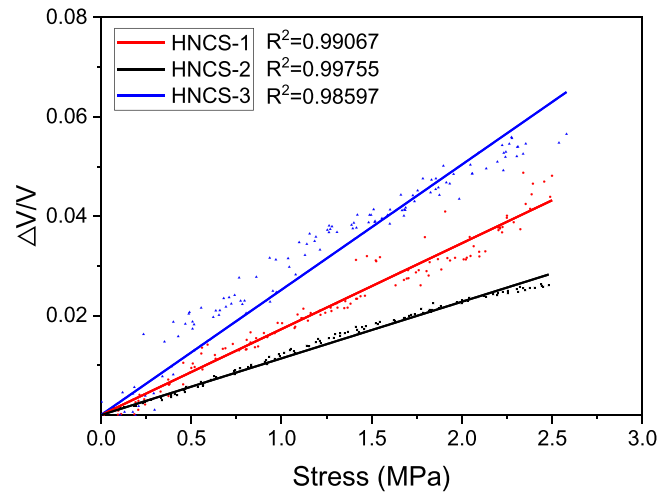


**Figure 7.** Pressure-sensitivity of the three HNCSs.

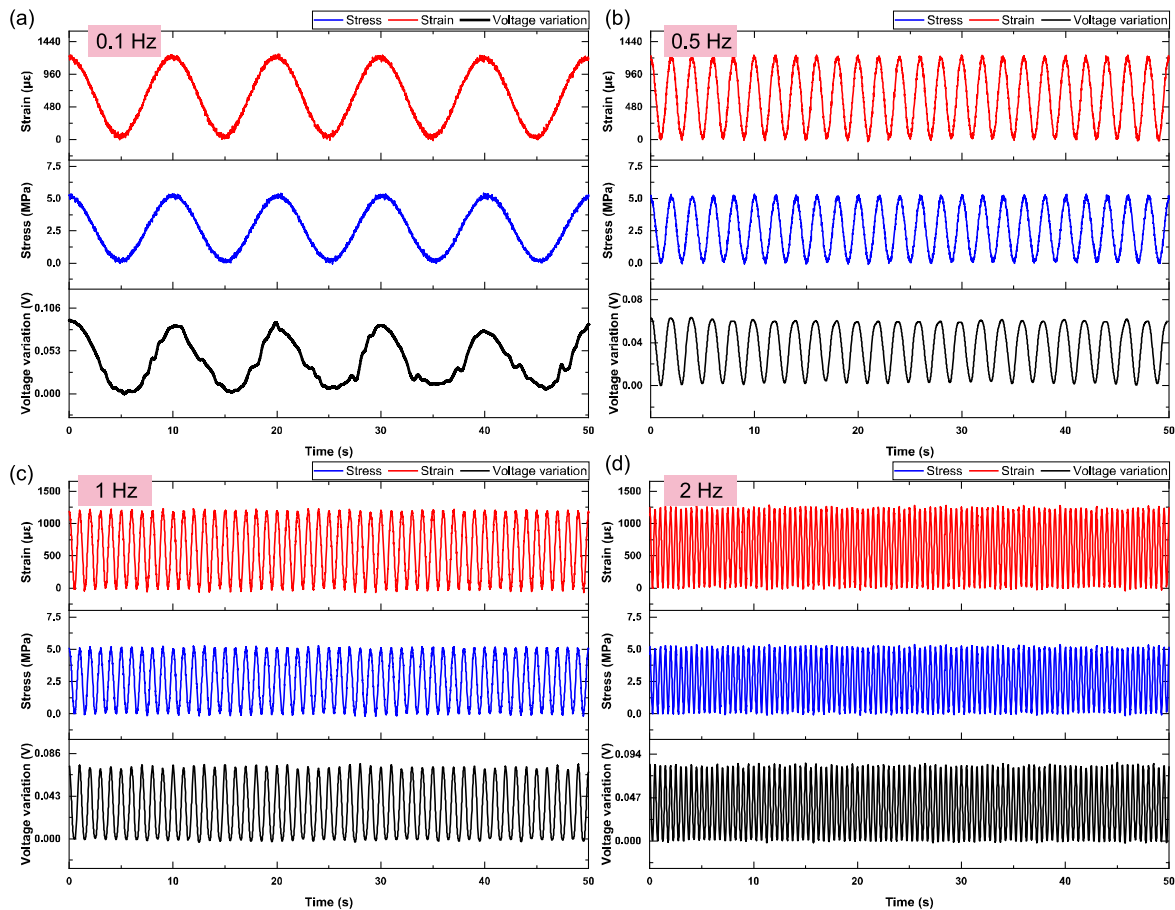


**Figure 8.** The voltage variation versus time curves and strain/stress versus time curves of the HNCS-1 under different loading frequencies: (a) 0.1 Hz; (b) 0.5 Hz; (c) 1.0 Hz; (d) 2.0 Hz.

investigate the torsional behavior of the model. A force transducer (TYPE8201, Brüel & Kjær, Denmark) is placed in series with the electromagnetic vibrator on the first floor to measure the control force for excitation and structural parameter identification.

Han *et al* [18] demonstrated that the HNCS can be made in bulk, coating, sandwich, bonded and embedded forms for

SHM applications. Compared with the other four forms, the bonded form can achieve higher monitoring efficiency and lower construction cost, in which the HNCS only lies in key positions of concrete component. In order for the HNCS to adhere to the building model, we have designed a special clamp, which consists of two L-shaped angle steel elements and two steel plates. A pair of screws is used to fix the

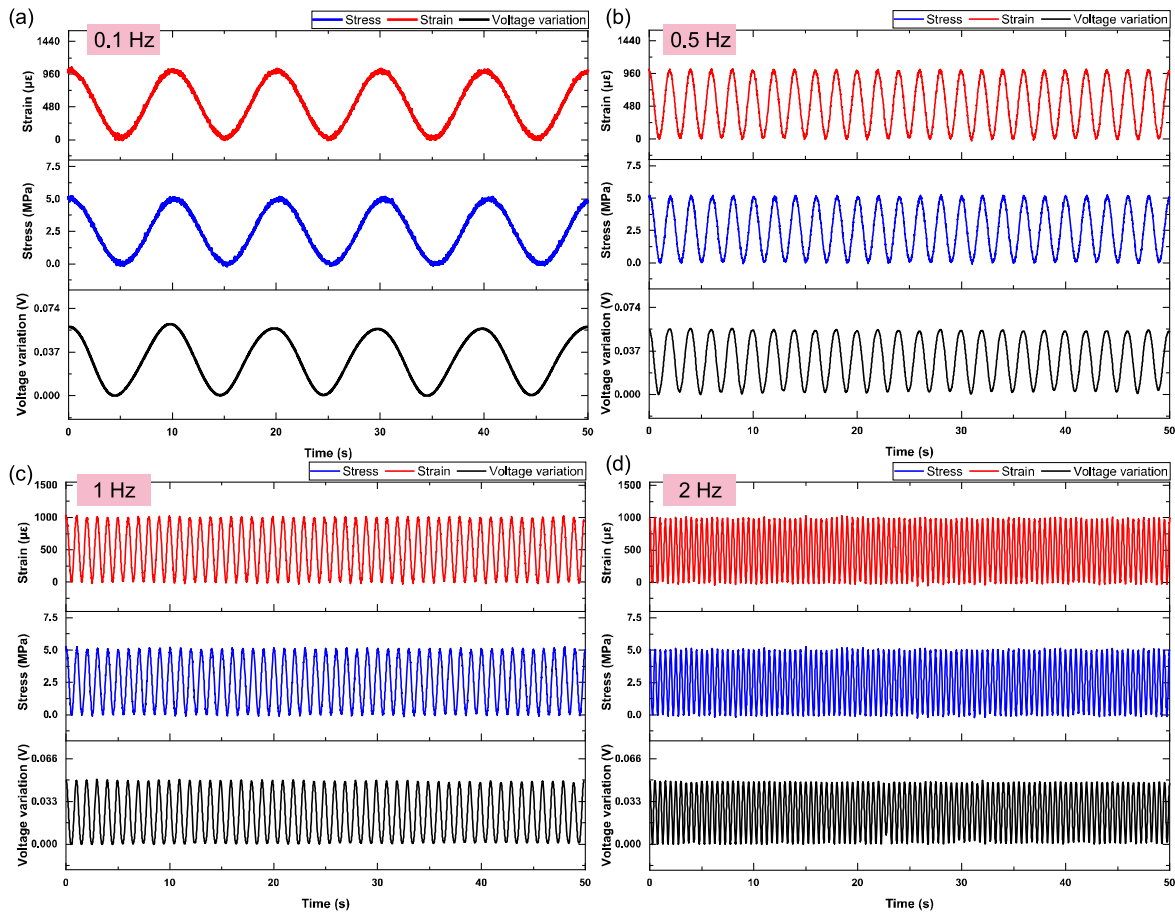


**Figure 9.** The voltage variation versus time curves and strain/stress versus time curves of the HNCS-2 under different loading frequencies: (a) 0.1 Hz; (b) 0.5 Hz; (c) 1.0 Hz; (d) 2.0 Hz.

L-shaped angle steel element on the steel plate as shown in figure 2(b). The HNCS is stuck between the two steel plates using a modified acrylic adhesive (DY-J39, Deyiglu, China) as shown in figure 2(c). This adhesive is based on methyl acrylate and can bond steel and concrete strongly within 10 min. It is also electrically insulative so that no additional insulative plate is needed to be placed between the HNCS and the steel plate to eliminate electrical interference. It should be noted that the side of the steel plate connected to the HNCS should be flat without holes to avoid screw hole clogging due to glue inflow. The HNCS-1, HNCS-2 and HNCS-3 are attached in the middle of the 1st, 3rd and 5th floor columns on the same side respectively using the same modified acrylic adhesive (figure 3(a)). In this way, the HNCSs can be compressed and stretched evenly without the need of an initial prestress when the dynamic excitation is executed. In addition, the proposed clamp provides the possibility to *in situ* replace the HNCSs conveniently without taking down the L-shaped angle steel from the column. Three strain gauges (BX120-5AA, Huangyan Testing Apparatus, China) are attached accordingly at the same locations of the HNCSs but the opposite side of the column. Two longitudinal strain gauges are also symmetrically deployed at the middle of the opposite lateral surface of each HNCS for comparison.

In this experiment, signals including strain, voltage, acceleration and force are collected simultaneously as shown in figure 2(a). It should be noted that the sensing property of the HNCS stems from the change of conductive network inside composite, and the volume electrical resistance/resistivity of the HNCS collected via the two-probe method or the four-probe method using multimeters is fully able and mostly used to characterize its sensing behavior due to simplicity. However, the commercially available multimeters generally have a relatively low sampling frequency (less than 50 Hz) and sensitivity, which limits the implementation of electrical resistance measurement of the HNCS in this study. In addition, the change in electrical resistivity  $\Delta\rho$  of the HNCS caused by deformation is the same as that in electrical resistance  $\Delta R$ , which is equal to the change in electrical voltage signal  $\Delta V$ , i.e.,

$$\Delta\rho/\rho = \Delta R/R = \Delta V/V, \quad (1)$$

where  $\rho$  is electrical resistivity of the HNCS,  $R$  is electrical resistance of the HNCS,  $V$  is voltage at both ends of the HNCS [33]. Therefore, voltage measurement approach is instead adopted by arranging a fixed resistor (100  $\Omega$ ) in series with each HNCS for voltage sharing. A DC regulated power supply (NP-9615, Manson, Hong Kong) is stabilized at 3 V to provide electrical input to the HNCS. As illustrated in

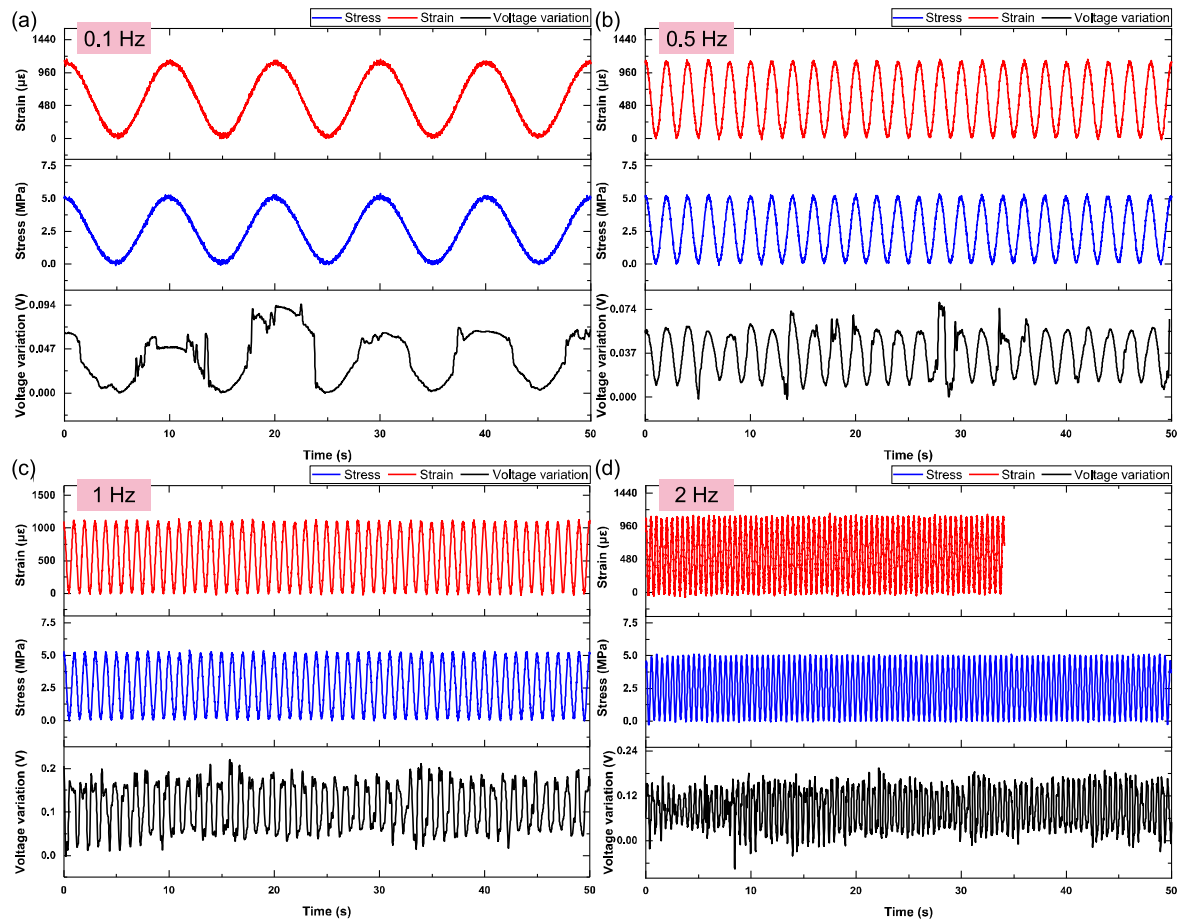


**Figure 10.** The voltage variation versus time curves and strain/stress versus time curves of the HNCS-3 under different loading frequencies: (a) 0.1 Hz; (b) 0.5 Hz; (c) 1.0 Hz; (d) 2.0 Hz.

figure 3(a), the voltage output of each HNCS, signals from the accelerometers and the force signal after being amplified by a charge amplifier (KD5008C, Kedong, China) are acquired simultaneously using a data acquisition system (SIRIUS, Dewesoft, Slovenia) powered by a commercial DewesoftX3 software. The voltage measurement sampling frequency can be as high as  $200 \text{ kS s}^{-1}$  with accuracy of  $\pm 0.1\%$  of reading  $\pm 0.02 \text{ V}$ . Signals from the strain gauges on the column and near the HNCSs are respectively measured using a dynamic data logger (EDX-100A, Kyowa, Japan) connected with two bridge boxes (DB-120T-8, Kyowa, Japan) via 1/4 bridge connection. Figure 3 shows the pictures of the experimental setup.

Before the structural vibration tests, the three HNCSs are calibrated and dynamically tested via a hydraulic material testing system (MTS810, MTS, USA). Here, the HNCSs bonded with two steel plates are taken out alone for compression testing as illustrated in figure 4. The data acquisition procedure is the same as mentioned above. The initial electrical resistances of the three HNCSs are also measured by two-probe method using a digital multimeter (DMM7510, Keithley, USA). For each HNCS, the electrical resistance is calculated by taking an average of five data collected after 300 s to mitigate the shift due to polarization effect.

### 2.3. Experimental tests

**2.3.1. Tests of static and dynamic performance of HNCS.** In sensor performance calibration, the HNCSs are firstly preformed under a quasi-statically axial compression operating under force control with loading rate of  $500 \text{ N min}^{-1}$ . With the aim of protecting the HNCSs and maintaining elastic deformation, the HNCSs are compressed in a very low force range (0–1000 N). Then, the dynamic performance of each HNCS is tested at different frequency values of 0.1, 0.5, 1.0 and 2.0 Hz to a sinusoidal load varying from 0 to 2000 N to verify the stability and repeatability of the HNCS. To mitigate the signal shift caused by polarization effect, each HNCS is firstly compressed at a constant load of 2000 N for 5 min and then imposed by the sinusoidal loads at different frequencies. The duration of each sinusoidal load is 50 s for all frequencies.

After sensor calibration, the HNCSs are deployed on a column of the building model and the dynamic performance of the HNCSs adhering to the building column is tested again under sinusoidal excitations generated by the electromagnetic vibrator. The excitation frequency is controlled to be 2, 6, 7, 10, 20 and 40 Hz for a duration of 20 s each through the

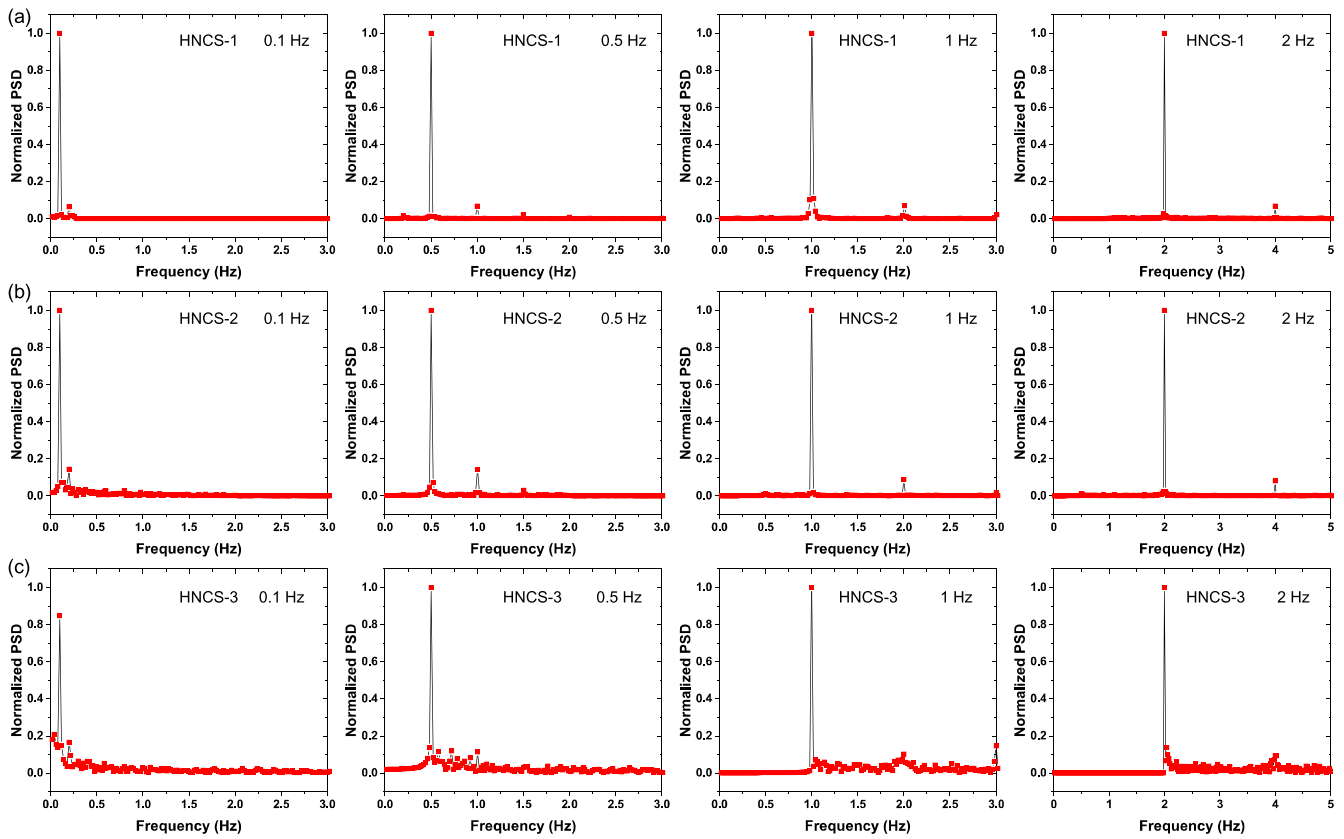


**Figure 11.** Normalized PSDs of voltage variations of the HNCSs under different loading frequencies. (a) HNCS-1; (b) HNCS-2; (c) HNCS-3.

signal generator. Here, the magnitude of excitations is not kept as a constant under different excitation frequencies because it is difficult to be exactly adjusted with the signal generator model used, especially when the frequencies are higher than 10 Hz.

**2.3.2. Tests for structural modal identification and damage detection.** To simulate different damage scenarios of the building model, two auxiliary iron bricks with different weights are respectively screwed in the center of floor plate by a long bolt as shown in figure 5(a). The weights of two bricks along with bolts are 7.635 kg (denoted as LB) and 12.590 kg (denoted as HB), respectively. The two bricks are placed at different floors to simulate different damage locations on the building model. For structural modal identification and damage detection, free-vibration experiments are conducted by exciting the building model via an impulse hammer. The acceleration response of each floor, the responses of the HNCSs and strain gauges at the 1st, 3rd and 5th floors are measured via a built-in anti-aliasing filter. A high-pass filter with 0.1 Hz AC coupling is applied to the voltage outputs of the HNCSs to eliminate the polarization shift. The modal parameters of the building model, including its natural frequencies and mode shapes, are identified after executing the Fast Fourier transform (FFT) with 2048 sampling points. The change in natural frequencies is used to detect the structural damage. The data processing procedure is illustrated in figure 5(b). The sampling rate for all the signals collected is 1000 Hz.

### 3. Results and discussion

#### 3.1. Sensor performance under quasi-static and dynamic loadings

To characterize the sensing performance of the as-prepared HNCSs, different loading scenarios are implemented. Figure 6 shows the stress–strain curves for the three HNCSs measured under a quasi-statically axial compression with an amplitude of 2.5 MPa. In order to protect the HNCSs, this value applied is far less than the typical compressive strength ( $\sim 30$  MPa in our previous work [42]) of cementitious composites with 6 wt% of CNT/NCB composite fillers. As shown in figure 6(a), the stress–strain curves for the three HNCSs show good linearity and appear to coincide well with each other, especially for HNCS-1 and HNCS-2. The elastic moduli obtained from linear fitting of the stress–strain curves are shown in figure 6(b). The elastic moduli of the three HNCSs are very close, indicating that the HNCSs have similar mechanical properties and the CNT/NCB composite fillers are uniformly dispersed in the composites (figure 1(b)). This observation can also be verified by the result that the electrical resistances of the HNCSs as listed in table 3 have the same order of magnitude. However, the elastic moduli of the three HNCSs are all less than that ( $\sim 9$  GPa) of the cementitious composite with 6 wt% of CNT/NCB composite fillers in our previous work [42]. This difference might be attributed to the relatively soft modified acrylic adhesive layers between the steel plates and the HNCS as well as different specimen dimensions.

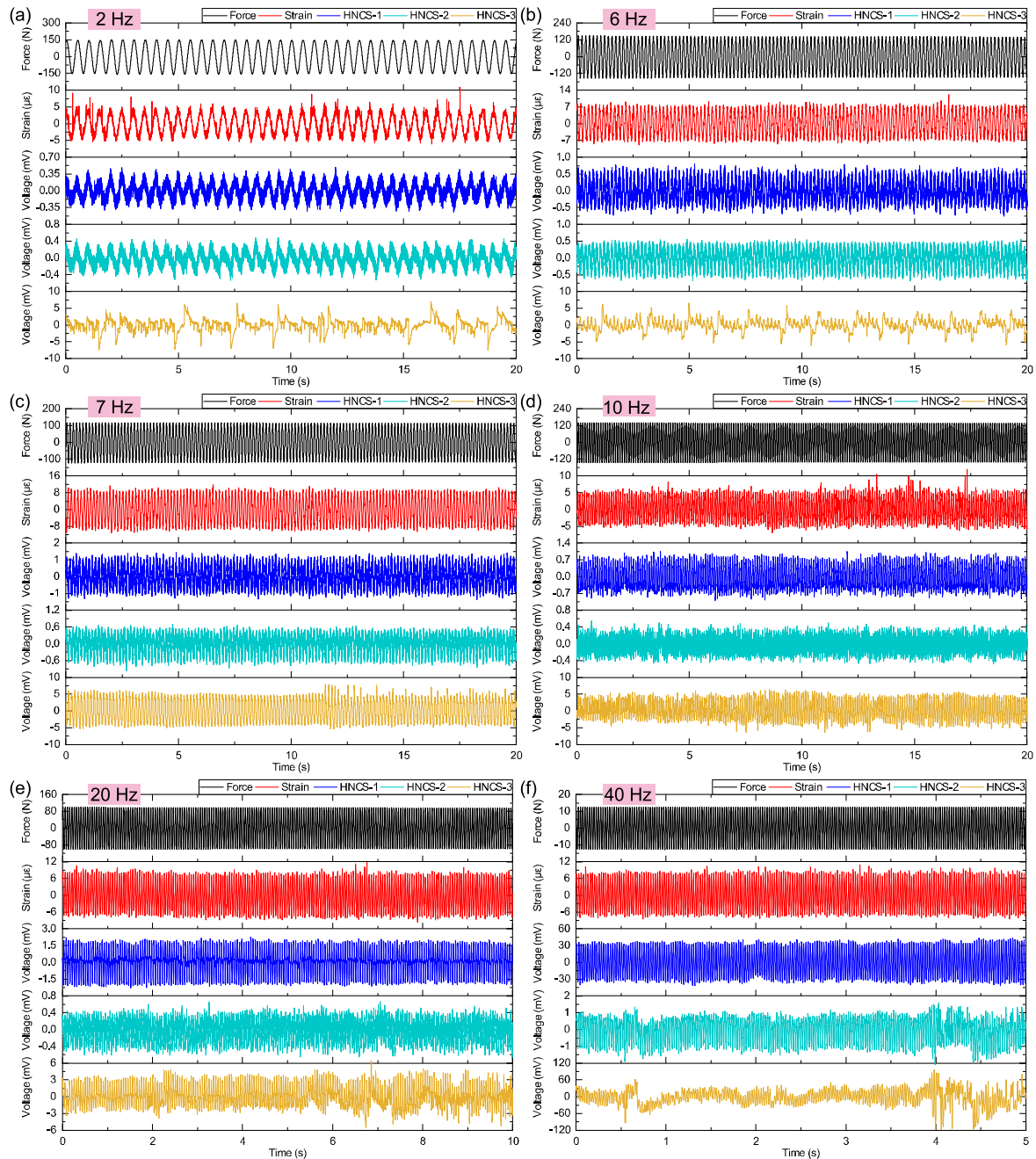


**Figure 12.** Dynamic responses of the HNCSSs attached on the building model as well as force sensor and strain gauge under different excitation frequencies: (a) 2 Hz; (b) 6 Hz; (c) 7 Hz; (d) 10 Hz; (e) 20 Hz; (f) 40 Hz.

The fractional change in voltage of the three HNCSSs as a function of the applied stress is shown in figure 7. The pressure-sensitivity  $S$  is given by

$$S = \frac{\Delta V/V}{\sigma}, \quad (2)$$

where  $\Delta V/V$  is the fractional change in voltage shared by the HNCSS and  $\sigma$  is the applied stress. As shown in table 3, the HNCSS-3 has a larger pressure-sensitivity (2.52%/MPa) compared to the HNCSS-1 (1.73%/MPa) and the HNCSS-2 (1.14%/MPa), which is similar to the trend of elastic modulus, indicating the potential dependence of elastic modulus

on pressure-sensitivity. It can also be seen from figure 7 that the HNCSS-1 ( $R^2 = 0.99067$ ) and HNCSS-3 ( $R^2 = 0.98597$ ) show worse linearity (i.e. pressure-sensitive stability) compared with the HNCSS-2 ( $R^2 = 0.99755$ ).

To better understand the pressure-sensitive stability of the HNCSSs, the dynamic performance of the HNCSSs is evaluated by imposing sinusoidal compressions at various frequencies, as shown in figures 8–10. It should be noted that loading frequencies higher than 2 Hz are not considered herein due to the limited displacement for the compression platen of the MTS machine in a cyclic period within such a low force range (0–2000 N). The HNCSSs responses are digitally detrended and filtered using ideal band-pass filters with cut-off frequencies of

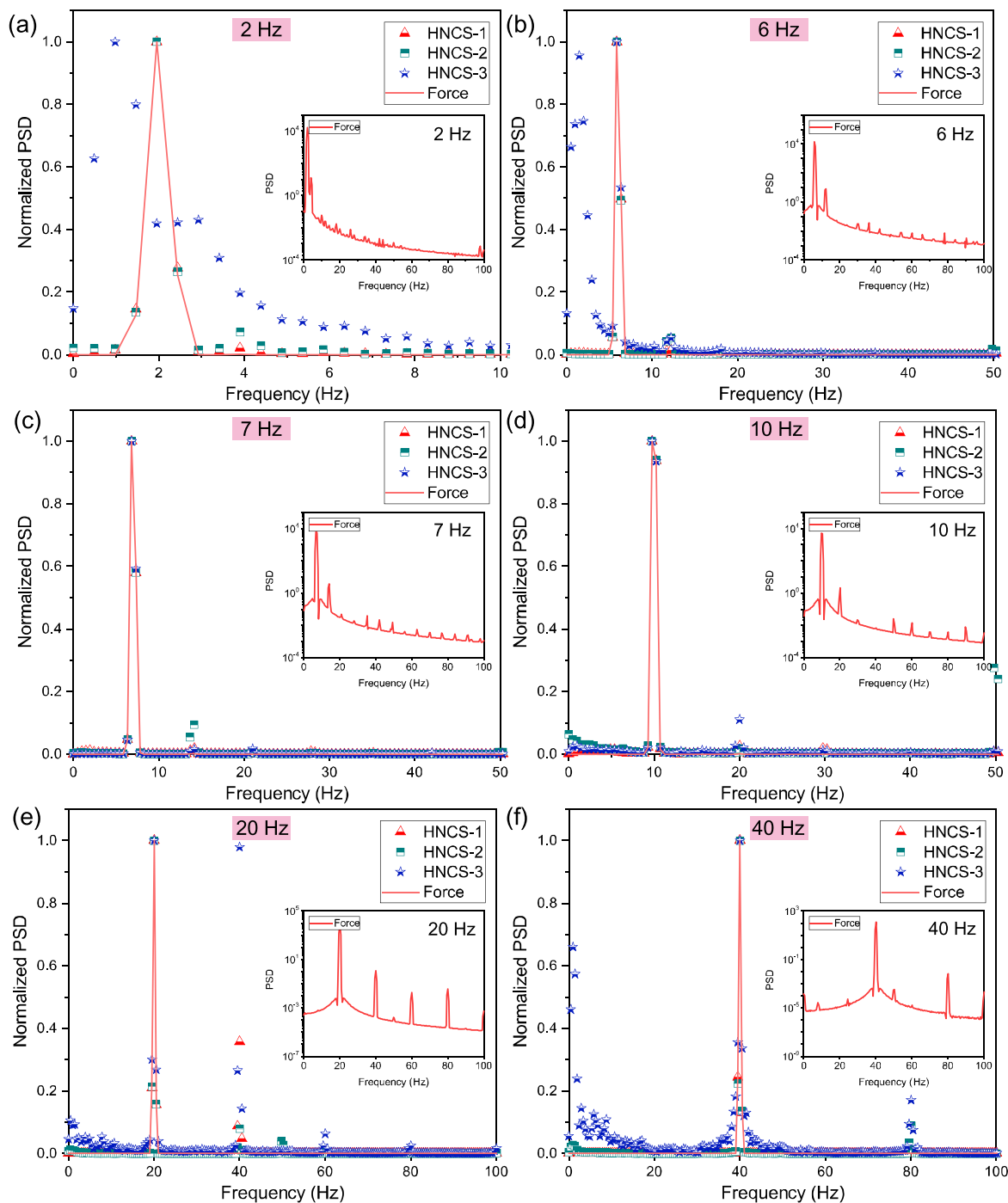


**Figure 13.** Frequencies measured by the HNCSs, benchmarked with the force sensor: (a) 2 Hz; (b) 6 Hz; (c) 7 Hz; (d) 10 Hz; (e) 20 Hz; (f) 40 Hz. The insets show the PSDs from the force sensor are re-plotted in logarithmic scale.

0.1 and 50 Hz to remove the polarization shift and undesired noises. As shown in figures 8–10, the voltage variation as a function of time shows a similar change trend with the time histories of the applied stress/strain, indicating superb response and recovery properties. In addition, different peak values (HNCS-2 < HNCS-1 < HNCS-3) are observed for the HNCSs at the same loading frequency, further verifying the different pressure-sensitivities under dynamic deformation of the three HNCSs, which is similar to the results observed in static deformation. However, the voltage variation of the HNCS-2 reaches

rapidly almost the same value in each cycle. Its peak values of voltage variation can accurately identify the amounts of the applied stress/strain, thus featuring the best pressure-sensitive reproducibility and stability at  $f = 0.1$  Hz compared with the other two. Especially for the HNCS-3, the voltage variation versus time curve is not smooth and symmetric with plenty of spikes and is inconsistent in the amplitudes. For the HNCS-1, the voltage variation versus time is not smooth with a few fluctuations only at loading frequency of 0.1 Hz. The curve becomes very smooth and has a good correlation between voltage

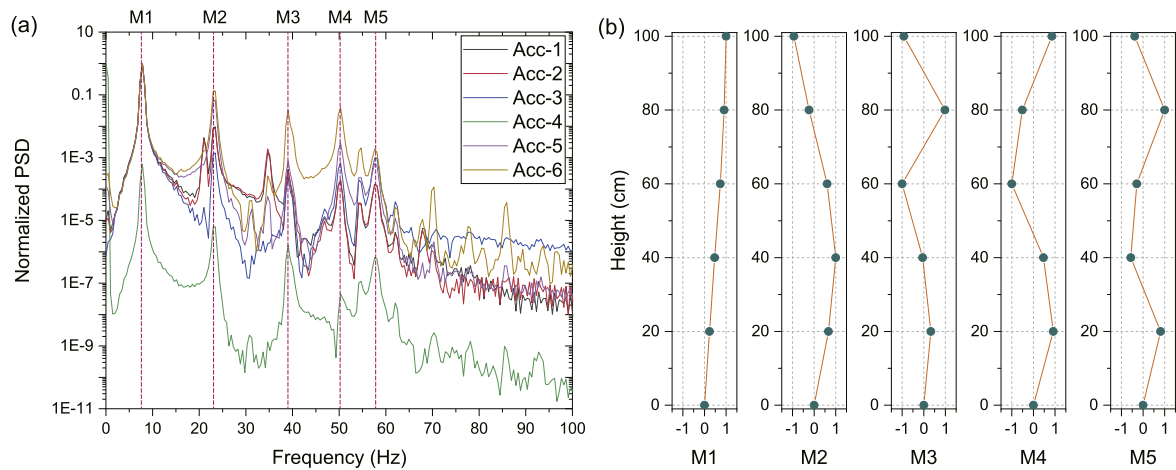


**Figure 14.** (a) Normalized PSDs of the responses measured by accelerometers in  $x$ -direction; (b) identified normalized mode shapes of first five modes in  $x$ -direction.

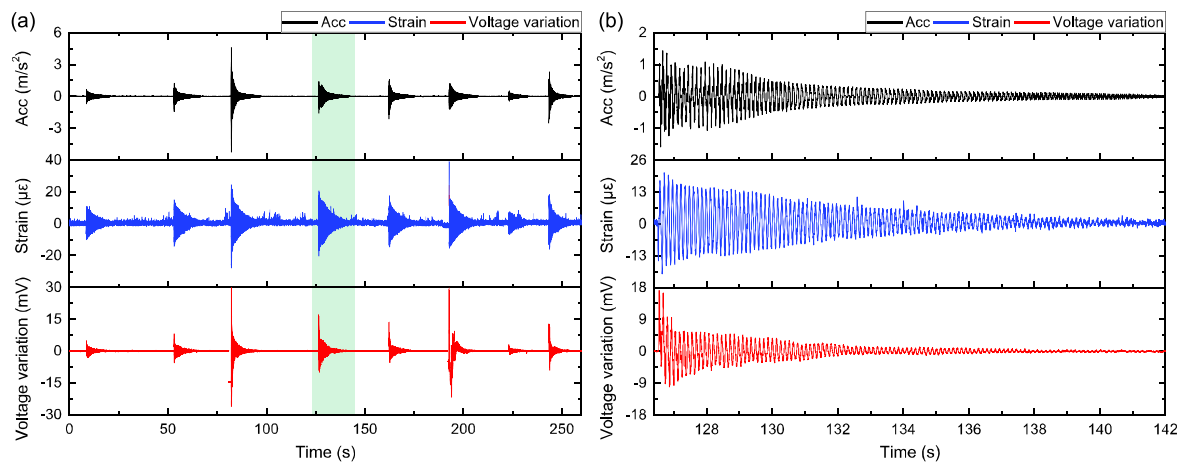


**Figure 15.** (a) Time histories of structural responses measured by accelerometer, strain gauge and HNCS-1 during hammer impact tests; (b) the enlarged response-decaying curves from the three types of sensors during a hammer impact test.

variation and stress/strain for loading frequencies higher than 0.1 Hz, demonstrating even better stability than the HNCS-2. Such good pressure-sensitive stability of the as-prepared HNCSs is attributed to three reasons: First, the applied stress is exactly within the elastic deformation range of the cementitious composites with CNT/NCB composite fillers [42]. The adjacent CNT/NCB composite fillers contact with each other, forming continuous conductive paths inside the cementitious composites. During deformation, the change of contact spots between the fillers and the change of intrinsic resistance of the fillers become the dominant factors of pressure-sensitivities. The conductive network inside the composite is stabilized, presenting steady sensing property [16]. Third, due to the specific feature of the CNT/NCB composite fillers, the conductive network formed inside the HNCSs is highly uniform, which benefits the pressure-sensitive stability. On the whole, the pressure-sensitive stabilities of the fabricated HNCSs are satisfactory and suitable for vibration

measurements and modal identification, which will be addressed in the following section. It is of note that the unsatisfactory performance of the HNCS-3 might be attributed to the weak bonding between the copper electrodes and the cementitious matrix, which should be further improved in the fabrication process.

Figure 11 shows the normalized power spectral densities (PSDs) of voltage variations of the HNCSs under different loading frequencies in line with figures 8–10. As illustrated, the dominant frequency identified by the three HNCSs coincides well with the applied loading frequency. However, the dynamic responses of the HNCSs are not monochromatic in the frequency domain, but rather contain super-harmonics at multiples of the applied loading frequency. Similar results have also been reported by García-Macías *et al* [43] and D'Alessandro *et al* [44]. In view of the small loading range, the super-harmonic responses of the HNCSs under cyclic loadings may not be related to nonlinearities, but to intrinsically time-varying nature of cement-based matrix [43, 44], in particular, of viscoelastic C-S-H gel. This behavior of the HNCSs may produce undesired frequency components when

applied for vibration-based SHM, which should be filtered out via post signal processing.

### 3.2. Dynamic performance of HNCSs attached on the building model

To further demonstrate the potential of HNCSs for vibration measurements, the dynamic performance of the as-prepared HNCSs attached on the building model is investigated using sinusoidal excitations with a frequency range from 2 to 40 Hz induced by the electromagnetic vibrator. In each sinusoidal vibration cycle, the HNCSs are cyclically compressed and stretched due to the periodic bending of the instrumented column. Figure 12 shows the outputs of the three HNCSs and the force sensor installed at the first floor level without any filtering. For comparison, the signal collected by the strain gauge glued to the column surface of the first story at the same cross section but opposite to the HNCS-1, is also presented in figure 12. It is worth noting that the excitation force, i.e. force input, is controlled by the real-time reading of the force sensor. It is observed that the outputs of the HNCS-1 and HNCS-2 coincide well with the applied force. The voltage variations are quickly increased when the HNCSs are compressed, and subsequently return to zero when the column returns to the initial state (straight). When the HNCSs are stretched, the voltage variations are rapidly increased to the same peak absolute value as compressed. However, the HNCS-3 shows irregular and hash response to the sinusoidal excitations when the frequency is lower than 6 Hz. At the frequencies higher than 20 Hz, both HNCS-2 and HNCS-3 produce undesirable fluctuations, and voltage variations at a certain force level are unstable with high noise level. By contrast, the HNCS-1 constantly performs stable at each frequency despite small strain amplitudes (less than  $10 \mu\epsilon$ ). The results are favorably consistent with the performance of the individual HNCSs under quasi-static and dynamic loadings without clamp holding. This confirms that the HNCSs can be well connected with the building model by using the devised clamps. It should be mentioned that the sensing properties of the HNCSs for compression and tension are assumed to be similar due to the small deformation range in this work. The devised clamps may not be well workable and pre-compression should be applied when the deformation at sensor location is large.

The normalized PSDs of the signals acquired by the HNCSs and the outputs of the force sensor are shown in figure 13. As illustrated, the normalized PSDs from the HNCS-1 and HNCS-2 are overlapped in coincidence with the normalized PSDs from the force sensor, indicating a good frequency identification. The HNCS-3 also presents qualified frequency responses at loading frequencies higher than 7 Hz in spite of its poor pressure-sensitive stability and high level of measurement noise. Some undesirable singular values multiple of the excitation frequency are also observed in each PSD plot, similar to the results given in section 3.1. It is worth mentioning that frequency multiplication generated by the electromagnetic vibrator may also be a cause for such super-harmonic responses in this study as it can be obviously

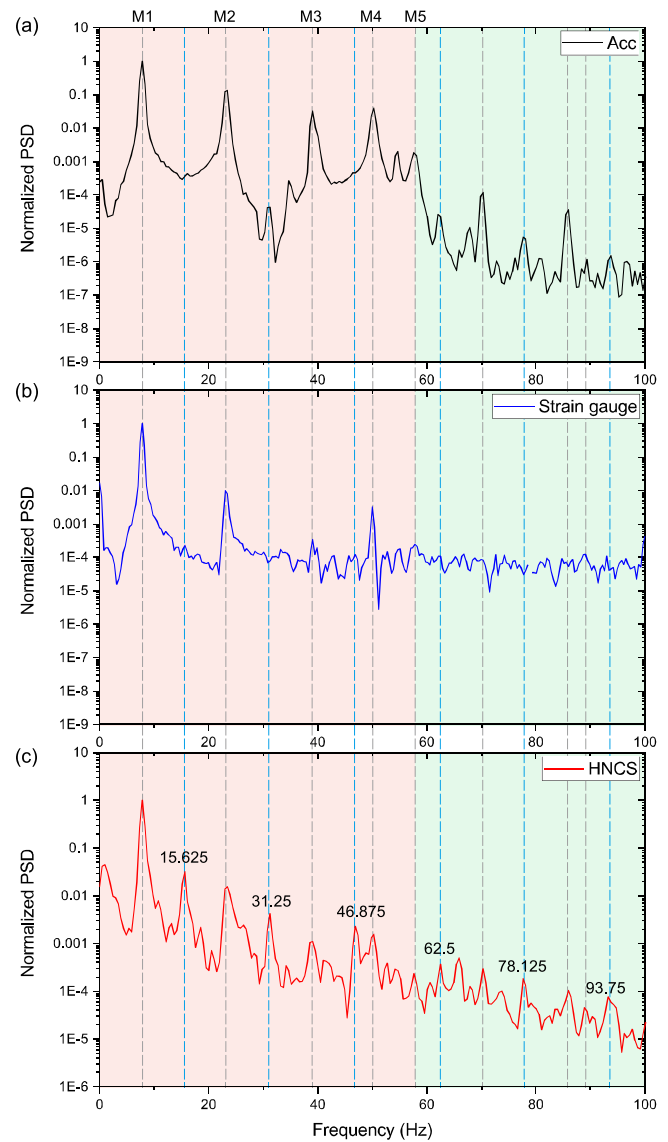


**Figure 16.** Identified modal frequencies using (a) accelerometer; (b) strain gauge; (c) HNCS-1. Red zone: first five modes; green zone: higher-frequency modes.

observed in the inserts of figure 13, where the PSDs from the force sensor are plotted on a logarithmic scale.

### 3.3. Structural modal identification and damage detection using HNCSs

It is known from the above tests that the HNCS-1 presents better sensing performance than the other two HNCSs. Therefore, for the sake of simplicity, only the HNCS-1 is employed as a sensor to acquire data for structural modal identification and damage detection. Modal-based methods use the change in natural frequencies as the basic feature for damage identification. Using the change in natural frequencies is attractive in that the frequencies can be conveniently identified through measuring a few accessible points on the structure and are usually less contaminated by noise. The modal identification is conducted using the frequency domain decomposition (FDD)

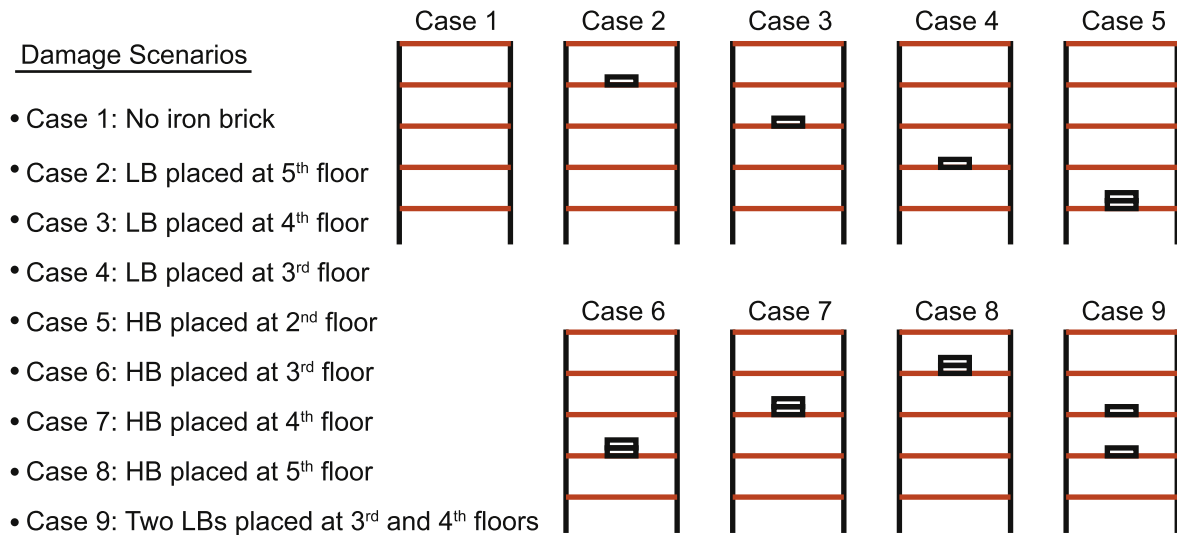


Figure 17. Simulated damage scenarios.

Table 4. Identified modal frequencies and their changes using accelerometer and the HNCS-1 in different damage scenarios.

| Damage case | Sensor | Natural frequency (Hz) |       |       |       |       | Natural frequency change (%) |       |       |       |       |
|-------------|--------|------------------------|-------|-------|-------|-------|------------------------------|-------|-------|-------|-------|
|             |        | M1                     | M2    | M3    | M4    | M5    | M1                           | M2    | M3    | M4    | M5    |
| 1           | Acc.   | 7.813                  | 23.93 | 40.04 | 51.76 | 58.59 | —                            |       |       |       |       |
|             | HNCS   | 7.813                  | 23.93 | 40.04 | 51.76 | 58.59 |                              |       |       |       |       |
| 2           | Acc.   | 7.813                  | 24.41 | 39.55 | 49.80 | 57.13 | 0                            | +2.01 | -1.22 | -3.79 | -2.49 |
|             | HNCS   | 7.813                  | 24.41 | 39.55 | 49.80 | 57.13 |                              |       |       |       |       |
| 3           | Acc.   | 7.813                  | 23.93 | 38.57 | 51.76 | 57.13 | 0                            | 0     | -3.67 | 0     | -2.49 |
|             | HNCS   | 7.813                  | 23.93 | 38.57 | 51.76 | 57.13 |                              |       |       |       |       |
| 4           | Acc.   | 7.813                  | 23.44 | 39.06 | 50.29 | 57.62 | 0                            | -2.05 | -2.45 | -2.84 | -1.66 |
|             | HNCS   | 7.813                  | 23.44 | 39.06 | 50.29 | 57.62 |                              |       |       |       |       |
| 5           | Acc.   | 7.813                  | 23.44 | 37.11 | 49.32 | 58.11 | 0                            | -2.05 | -7.32 | -4.71 | -0.82 |
|             | HNCS   | 7.813                  | 23.44 | 37.11 | 49.32 | 58.11 |                              |       |       |       |       |
| 6           | Acc.   | 7.813                  | 22.46 | 39.55 | 49.32 | 57.62 | 0                            | -6.14 | -1.22 | -4.71 | -1.66 |
|             | HNCS   | 7.813                  | 22.46 | 39.55 | 49.32 | 57.62 |                              |       |       |       |       |
| 7           | Acc.   | 7.813                  | 23.44 | 38.09 | 51.76 | 56.15 | 0                            | -2.05 | -4.87 | 0     | -4.17 |
|             | HNCS   | 7.813                  | 23.44 | 38.09 | 51.76 | 56.15 |                              |       |       |       |       |
| 8           | Acc.   | 7.813                  | 24.41 | 39.55 | 48.83 | 56.64 | 0                            | -2.01 | -1.22 | -5.66 | -3.33 |
|             | HNCS   | 7.813                  | 24.41 | 39.55 | 48.83 | 56.64 |                              |       |       |       |       |
| 9           | Acc.   | 7.813                  | 22.95 | 38.57 | 50.78 | 56.64 | 0                            | -4.10 | -3.67 | -1.89 | -3.33 |
|             | HNCS   | 7.813                  | 22.95 | 38.57 | 50.78 | 56.64 |                              |       |       |       |       |

technique, which is based on the fact that well separated modes can be estimated directly from the PSD matrix at the peaks [45].

Figure 14(a) shows the normalized PSD spectra of the structural responses measured by the six accelerometers during the hammer tests. Obviously, five peaks are simultaneously observed in the six PSD spectrum curves in the frequency range below 60 Hz, denoted as M1, M2, M3, M4 and M5 respectively; and the first mode is at 7.813 Hz, which is the fundamental frequency of the building model in the weak-axis direction ( $x$ -direction). Figure 14(b) illustrates the identified mode shapes of the five modes, which are elicited by a blind modal identification method based on the second-order statistic [46].

Figure 15(a) shows the time histories of the measured acceleration (from the accelerometer close to the HNCS-1), strain response and voltage variation during hammer impact tests. The strain signal is obtained by taking an average of the outputs from the two strain gauges positioned in the vicinity of the HNCS-1. It is apparent that the three different types of sensors react to the impact simultaneously, varying with the different impact intensities. The enlarged free vibration decaying curves of the three types of sensors to a single hammer impact are plotted in figure 15(b). The signal from the HNCS-1 is gradually attenuated over time, showing a low noise level and a comparatively long decay time, which makes it proper to be used for damping estimation. To verify

the authenticity of the responses, the modal frequencies are identified using the data from the three different types of sensors. It can be observed from figure 16 that the identified modal frequencies from the HNCS-1 are highly consistent with their counterparts determined from the accelerometer and strain gauge. In addition, the HNCS-1 offers more high-frequency components than the strain gauge, which is explained by a higher noise level from the latter in strain measurements. However, a peak at 15.625 Hz between M1 and M2 is also observed in figure 16(c), which might be a resonant frequency related to y-direction as the HNCS-1 is placed at a column of the building model, not at a neutral position that only senses vibrations in x-direction. This may also explain other extra peaks compared with the outputs of the accelerometer and strain gauge. Similarly, the super-harmonics at 15.625 Hz, 31.25 Hz, and other multiples of 15.625 Hz are observed in the output spectrum of the HNCS-1, which confirms the harmonic distortion behavior of the HNCS-1.

Since extra mass can lead to a change in structural properties, the damage in this study is simulated by attaching additional masses. One advantage of such damage pattern is that the structural stiffness remains unchanged while the mass is altered. Another merit is the ease of changing the location and severity of damage. As shown in figure 17, in this experiment, nine scenarios including one healthy state and eight damaged states are considered. In Case 1, the structure is healthy; in Cases 2–5, a light iron brick is bolted tightly to the center of the 5th floor, 4th floor, 3rd floor and 2nd floor, respectively; in Cases 6–8, a heavy iron brick is bolted tightly to the center of the 3rd floor, 4th floor and 5th floor, respectively; In Case 9, the 3rd floor and 4th floor are simultaneously equipped with a light iron brick each. The identified modal frequencies in each scenario are illustrated in table 4. Changes in the modal parameters are not the same for each mode since the changes depend on the nature, location and severity of the damage. It is found that the results from the HNCS-1 are perfectly consistent with them from the accelerometer without any difference being observed, indicating that the HNCS-1 is sensitive enough to capture the dynamic response of the structure and applicable to structural health monitoring. Note that the vibration modes higher than the first one have increased sensitivity to local damage, which should be used in damage detection to attain a higher level of identification precision.

#### 4. Conclusions

This study presented a novel cement-based sensor fabricated with self-sensing cementitious composites for structural modal identification and modal-based damage detection. The HNCS made of self-sensing cementitious composites filled with CNT/NCB composite fillers was developed with an optimal content of CNT/NCB composite fillers and sensor dimension. The sensing performance of the as-made HNCSs under static and dynamic loadings was characterized. The HNCSs were then attached on a five-story building model via tailor-made L-shaped clamps to investigate their potential for

dynamic response monitoring and modal identification. The main conclusions of this study are summarized as follows.

- (1) The HNCSs containing CNT/NCB composite fillers have satisfactory mechanical property and close electrical resistance due to the uniform distribution of CNT/NCB composite fillers in the cementitious composites;
- (2) The voltage-sensed approach is suitable to characterize the sensing behavior of the HNCSs at high input frequencies due to its faster sampling rate and higher sensitivity with respect to common electrical resistance measurement. Under dynamic compression, the responses of the HNCSs as a function of time show a similar variation pattern as the time histories of the applied stress/strain, indicating excellent pressure-sensitive reproducibility and stability despite different pressure-sensitivities between the three HNCSs;
- (3) In comparison with the HNCS-2 and HNCS-3, the HNCS-1 constantly performs stable under sinusoidal excitations in the frequency range from 2 to 40 Hz, which is favorably consistent with the dynamic performance of the HNCSs without clamp holding, confirming that the HNCSs can be well connected with the building model by using the devised clamps. In addition, the normalized PSDs of the signals from the HNCSs are overlapped in coincidence with the normalized PSDs from the force sensor over the entire frequency range investigated, indicating the capability to identify the input frequency;
- (4) In the hammer tests, the identified modal frequencies from the HNCS-1 are highly consistent with their counterparts determined from the accelerometer and strain gauge. In addition, the HNCS-1 offers more high-frequency components than the strain gauge. The identified modal frequencies and their changes in various damage cases obtained by the HNCS-1 are perfectly consistent with those obtained by the accelerometer, indicating that the HNCS-1 is sensitive enough to capture dynamic response and applicable to structural health monitoring.

Future research efforts will be devoted to studying the long-term durability and stability of the HNCSs when they are permanently deployed on a structure. In addition, the possibility to spontaneously detect structural damage by self-sensing cementitious composites used in bulk form through vibration monitoring will be addressed. The issue of unsatisfactory signal quality of the HNCSs caused by the weak electrode-matrix bonding will also be resolved through optimized design of the fabrication process.

#### Acknowledgments

The work described in this paper was supported by a grant (TRS) from the Research Grants Council of the Hong Kong Special Administrative Region, China (Project No. T22/502/18), a grant from the National Science Foundation of China (51578110), and a grant from The Hong Kong Polytechnic

University (Project No. 1-BBAG). The authors would also like to appreciate the funding support by the Innovation and Technology Commission of the Hong Kong SAR Government (Project No. K-BBY1).

## ORCID iDs

Siqi Ding  <https://orcid.org/0000-0002-7565-4549>  
 You-Wu Wang  <https://orcid.org/0000-0003-2293-4712>  
 Yi-Qing Ni  <https://orcid.org/0000-0003-1527-7777>  
 Baoguo Han  <https://orcid.org/0000-0002-7081-3221>

## References

- [1] Sohn H and Law K H 1997 A Bayesian probabilistic approach for structure damage detection *Earthq. Eng. Struct. Dyn.* **26** 1259–81
- [2] Beck J L and Au S K 2002 Bayesian updating of structural models and reliability using Markov chain Monte Carlo simulation *J. Eng. Mech.* **128** 380–91
- [3] Ren W X and De Roeck G 2002 Structural damage identification using modal data: II. Test verification *J. Struct. Eng.* **128** 96–104
- [4] Bernal D and Gunes B 2004 Flexibility based approach for damage characterization: benchmark application *J. Eng. Mech.* **130** 61–70
- [5] Worden K and Dulieu-Barton J M 2004 An overview of intelligent fault detection in systems and structures *Struct. Health Monit.* **2** 85–98
- [6] Catbas F N, Brown D L and Aktan A E 2006 Use of modal flexibility for damage detection and condition assessment: case studies and demonstrations on large structures *J. Struct. Eng.* **132** 1699–712
- [7] Lynch J P and Loh K J 2006 A summary review of wireless sensors and sensor networks for structural health monitoring *Shock Vib. Dig.* **38** 91–128
- [8] Friswell M I 2007 Damage identification using inverse methods *Phil. Trans. R. Soc. A* **365** 593–410
- [9] Yang Y and Nagarajaiah S 2014 Structural damage identification via a combination of blind feature extraction and sparse representation classification *Mech. Syst. Signal Process.* **45** 1–23
- [10] Ko J and Ni Y 2005 Technology developments in structural health monitoring of large-scale bridges *Eng. Struct.* **27** 1715–25
- [11] Farrar C R, Park G, Allen D W and Todd M D 2006 Sensor network paradigms for structural health monitoring *Struct. Control Health Monit.* **13** 210–25
- [12] Brownjohn M W 2007 Structural health monitoring of civil infrastructure *Phil. Trans. R. Soc. A* **365** 589–622
- [13] Lynch J P, Wang Y, Sundararajan A, Law K H and Kiremidjian A S 2007 Wireless sensing for structural health monitoring of civil infrastructures *Struct. Infrastruct. Eng.* **3** 103–20
- [14] Nagayama T, Sim S H, Miyamori Y and Spencer B F Jr 2007 Issues in structural health monitoring employing smart sensors *Smart Struct. Syst.* **3** 299–320
- [15] Ni Y Q, Xia Y, Liao W Y and Ko J M 2009 Technology innovation in developing the structural health monitoring system for Guangzhou New TV Tower *Struct. Control Health Monit.* **16** 73–98
- [16] Ou J and Li H 2010 Structural health monitoring in mainland China: review and future trends *Struct. Health Monit.* **9** 219–31
- [17] Yun C B, Lee J J and Koo K Y 2011 Smart structure technologies for civil infrastructures in Korea: recent research and applications *Struct. Infrastruct. Eng.* **7** 673–88
- [18] Han B, Ding S and Yu X 2015 Intrinsic self-sensing concrete and structures: a review *Measurement* **59** 110–28
- [19] Li G Y, Wang P M and Zhao X 2007 Pressure-sensitive properties and microstructure of carbon nanotube reinforced cement composites *Cem. Concr. Compos.* **29** 377–82
- [20] Howser R, Dhonde H and Mo Y 2011 Self-sensing of carbon nanofiber concrete columns subjected to reversed cyclic loading *Smart Mater. Struct.* **20** 85031
- [21] Monteiro A O, Costa P M F J, Oeser M and Cachim P B 2020 Dynamic sensing properties of a multifunctional cement composite with carbon black for traffic monitoring *Smart Mater. Struct.* **29** 025023
- [22] Sun S, Ding S, Han B, Dong S, Yu X, Zhou D and Ou J 2017 Multi-layer graphene-engineered cementitious composites with multifunctionality/intelligence *Composites B* **129** 221–32
- [23] Konsta-Gdoutos M S, Danoglidis P A, Falara M G and Nitodas S F 2017 Fresh and mechanical properties, and strain sensing of nanomodified cement mortars: the effects of MWNT aspect ratio, density and functionalization *Cem. Concr. Compos.* **82** 137–51
- [24] Song C and Choi S 2017 Moisture-dependent piezoresistive responses of CNT-embedded cementitious composites *Compos. Struct.* **170** 103–10
- [25] Materazzi A L, Ubertini F and D'Alessandro A 2013 Carbon nanotube cement-based transducers for dynamic sensing of strain *Cem. Concr. Compos.* **37** 2–11
- [26] Galao O G, Baeza F J, Zornoza E and Garcés P 2014 Strain and damage sensing properties on multifunctional cement composites with CNF admixture *Cem. Concr. Compos.* **46** 90–8
- [27] García-Macías E and Ubertini F 2019 Earthquake-induced damage detection and localization in masonry structures using smart bricks and Kriging strain reconstruction: a numerical study *Earthq. Eng. Struct. Dyn.* **48** 548–69
- [28] Chen P W and Chung D D L 1993 Carbon fiber reinforced concrete for smart structures capable of non-destructive flaw detection *Smart Mater. Struct.* **2** 22–30
- [29] Esawi A M K and Farag M M 2007 Carbon nanotube reinforced composites: potential and current challenges *Mater. Des.* **28** 2394–401
- [30] De Volder M F, Tawfick S H, Baughman R H and Hart A J 2013 Carbon nanotubes: present and future commercial applications *Science* **339** 535–9
- [31] Li G Y, Wang P M and Zhao X 2005 Mechanical behavior and microstructure of cement composites incorporating surface-treated multi-walled carbon nanotubes *Carbon* **43** 1239–45
- [32] Yu X and Kwon E 2009 A carbon nanotube/cement composite with piezoresistive properties *Smart Mater. Struct.* **18** 1–5
- [33] Han B, Zhang K, Yu X, Kwon E and Ou J 2012 Electrical characteristics and pressure-sensitive response measurements of carboxyl MWNT/cement composites *Cem. Concr. Compos.* **34** 794–800
- [34] Cui X, Han B, Zheng Q, Yu X, Dong S, Zhang L and Ou J 2017 Mechanical properties and reinforcing mechanisms of cementitious composites with different types of multiwalled carbon nanotubes *Composites A* **103** 131–47
- [35] Garcia-Macias E, D'Alessandro A, Castro-Triguero R, Perez-Mira D and Ubertini F 2017 Micromechanics modeling of the electrical conductivity of carbon nanotube cement-matrix composites *Composites B* **108** 451–69

- [36] Han B, Yu X and Kwon E 2009 A self-sensing carbon nanotube/cement composite for traffic monitoring *Nanotechnology* **20** 445501
- [37] Howser R N, Dhonde H B and Mo Y L 2011 Self-sensing of carbon nanofiber concrete columns subjected to reversed cyclic loading *Smart Mater. Struct.* **20** 085031
- [38] Downey A, D'Alessandro A, Ubertini F and Laflamme S 2018 Automated crack detection in conductive smart-concrete structures using a resistor mesh model *Meas. Sci. Technol.* **29** 035107
- [39] Downey A, D'Alessandro A, Baquera M, García-Macías E, Rolfes D, Ubertini F, Laflamme S and Castro-Triguero R 2017 Damage detection, localization and quantification in conductive smart concrete structures using a resistor mesh model *Eng. Struct.* **148** 924–35
- [40] Ubertini F, Materazzi A L, D'Alessandro A and Laflamme S 2014 Natural frequencies identification of a reinforced concrete beam using carbon nanotube cement-based sensors *Eng. Struct.* **60** 265–75
- [41] Zou B, Chen S J, Korayem A H, Collins F, Wang C M and Duan W H 2015 Effect of ultrasonication energy on engineering properties of carbon nanotube reinforced cement pastes *Carbon* **85** 212–20
- [42] Han B, Wang Y, Ding S, Yu X, Zhang L, Li Z and Ou J 2017 Self-sensing cementitious composites incorporated with botryoid hybrid nano-carbon materials for smart infrastructures *J. Intell. Mater. Syst. Struct.* **28** 699–727
- [43] García-Macías E, Downey A, D'Alessandro A, Castro-Triguero R, Laflamme S and Ubertini F 2017 Enhanced lumped circuit model for smart nanocomposite cement-based sensors under dynamic compressive loading conditions *Sensors Actuators A* **260** 45–57
- [44] D'Alessandro A, Ubertini F, Materazzi A L, Laflamme S and Porfiri M 2015 Electromechanical modelling of a new class of nanocomposite cement-based sensors for structural health monitoring *Struct. Heal. Monit.* **14** 137–47
- [45] Salawu O S and Williams C 1995 Review of full-scale dynamic testing of bridge structures *Eng. Struct.* **17** 113–21
- [46] McNeill S I and Zimmerman D C 2008 A framework for blind modal identification using joint approximate diagonalization *Mech. Syst. Signal Process.* **22** 1526–48